Anang *et al. Water Emerg Contam Nanoplastics* 2023;2:3
DOI: 10.20517/wecn.2023.04

Water Emerging Contaminants & Nanoplastics

Research Article

Open Access

Check for updates

An insight into the fate of Cu^{2+} and zero-valent iron during removal of Cu^{2+} by nanoscale zero-valent iron

Emmanuella Anang[1], Hong Liu[1,2], Xianyuan Fan[1,2]

[1]College of Resource and Environmental Engineering, Wuhan University of Science and Technology, Wuhan 430081, Hubei, China.
[2]Hubei Key Laboratory for Efficient Utilization and Agglomeration of Metallurgic Mineral Resources, Wuhan University of Science and Technology, Wuhan 430081, Hubei, China.

Correspondence to: Prof. Hong Liu. College of Resource and Environmental Engineering, Wuhan University of Science and Technology, 115 Rookie Street, WUST, Wuhan 430081, Hubei, China. E-mail: liuhong64@126.com

How to cite this article: Anang E, Liu H, Fan X. An insight into the fate of Cu^{2+} and zero-valent iron during removal of Cu^{2+} by nanoscale zero-valent iron. *Water Emerg Contam Nanoplastics* 2023;2:3. https://dx.doi.org/10.20517/wecn.2023.04

Received: 10 Jan 2023 **First Decision:** 28 Feb 2023 **Revised:**14 Mar 2023 **Accepted:** 22 Mar 2023 **Published**: 31 Mar 2023

Academic Editor: Hafiz M.N. Iqbal **Copy Editor:** Ke-Cui Yang **Production Editor:** Ke-Cui Yang

Abstract

Aim: The transformation of zero-valent iron (Fe^0) and Cu^{2+} during Cu^{2+} removal by nanoscale zero-valent iron (nZVI) has not been properly investigated using modern analytical techniques, despite its importance in environmental toxicology and surface chemistry associated with wastewater treatment/groundwater remediation. This study critically examines the phenomenon using a variety of modern instruments that characterize the physical and chemical properties of materials and provides extensive comprehension of the subject.

Methods: As-prepared nZVI was used to remove Cu^{2+} in 5 mmol/L $CuSO_4$. The morphological and structural characteristics of the Cu^{2+} and nZVI after removal were investigated with the aid of scanning electron microscopy (SEM), transmission electron microscopy (TEM), X-ray diffraction (XRD) and X-ray photoelectron spectrometry (XPS).

Results: Complete removal of Cu^{2+} by the nZVI was achieved within 60 min and remained constant till 120 min. The Cu^{2+} got reduced into cuprite (Cu_2O) and copper metal (Cu^0) (the crystals of both transformation products were cubic), while the Fe^0 nanoparticles transformed into lath-like lepidocrocite (γ-FeOOH) and twin-rod goethite (α-FeOOH). The mechanism of Fe^0 transformation was that the Fe^{2+} produced by Fe^0 corrosion and oxidation by Cu^{2+} was hydrolyzed and oxidized to form hydropyrite, which was later converted into lepidocrocite and goethite

with the assistance of Fe^{2+}. The transformation of Cu^{2+} was due to the strong reduction property of Fe^{0}. The toxicity and bioavailability of the transformed products were lower than those of Cu^{2+} and Fe^{0} nanoparticles.

Conclusion: The findings are critical in understanding the fate of Fe^{0} nanoparticles and Cu^{2+} during Cu^{2+} removal by nZVI and can provide guidance for the application of nZVI technology.

Keywords: Removal efficiency, transformational products, heavy metal, nanoparticles

INTRODUCTION

Anthropogenic activities such as mining and galvanizing are the significant contributors to large concentrations of copper in the environment[1-3]. Even though copper is an essential trace element in living organisms, its excessive concentration is detrimental to life[4]. High concentrations of copper may cause dermatitis, nausea, cancer, chronic asthma, peritonitis, gastroenteritis, and growth retardation in humans[5-7]. The adverse effects on aquatic and plant life may be lethal and retard crop growth, respectively[5,6]. Considering the high toxicity and lethal effects of copper on life, several researchers have proposed many effective ways of removing copper from wastewater and groundwater[3,8-14]. Among the proposed removal techniques (ion exchange, adsorption, complexation, electrodialysis, membrane technology, bioremediation, solvent extraction and chemical treatment), nanotechnology is the most efficient and effective[15-19]

Nanoscale zero-valent iron (nZVI) has been employed extensively to remove contaminants such as dyes[20,21], nitrates[22,23], heavy metals[24-27], chloro-organic compounds[28-30], chlorinated pesticides and organophosphates[31,32] from wastewater and groundwater. Its removal mechanisms during reaction with heavy metals include adsorption (Zn, Cd, Ni, Pb, Cr, Co, Se, Ba, U, As), reduction (Cu, U, As, Pt, Hg, Ni, Ag, Pb, Cr), precipitation (Cd, Cu, Pb, Co, Zn), co-precipitation (Cd, Co, Cu, Zn, Pb), oxidation (Se, Pb, As, U), chemisorption and diffusion through pores[33-35].

The influence of environmental factors such as pH, dissolved oxygen and co-existing ions on the removal by nZVI has been investigated by previous researchers[36-38], but the transformation that nZVI undergoes when removing contaminants is understudied. Similarly, the transformations that the contaminants undergo during removal are not properly investigated through modern analytical techniques. A critical investigation of the transformation of nZVI and heavy metals in water is essential because of their potential evolution into more toxic substances after the treatment process. The evolution of heavy metals and nZVI into toxic substances have the potential to affect the environment and human health adversely (in the event that the toxic substances get into the food chain)[39]. Therefore, establishing the transformation products of zero-valent iron (Fe^{0}) and Cu^{2+} ions during nZVI application in Cu^{2+} removal and establishing their toxicity levels in the environment are equally essential in understanding ZVI technology and toxicity. Additionally, the exact mechanism through which Fe^{0} is transformed during the reaction, as well as the contributing factors to the transformation rate, remain debatable, particularly in the presence of different heavy metal ions. A previous study by Yang *et al.*[40] on the transformation of ferrihydrite (from Fe^{0} evolution) to magnetite or goethite showed that the variations in transformation rates cannot be entirely explained by the extent of Fe^{2+} sorption. Yang *et al.*[40] suggested that the rate of Fe^{2+} uptake by a solid is most important in determining the transformation of Fe^{x} species. The phenomenon can be likened to the assumption that heavy metal ions present in wastewater have a direct effect on the transformation rate of Fe^{0} to Fe^{2+}. In the investigation of the current study, we used analytical methods to characterize the changes in Fe^{0} reducibility and also demonstrated the transformational mechanism of Fe^{0} during reaction with Cu^{2+}.

In this study, Cu^{2+} was selected as the target heavy metal ion because of its prevalence in the environment and high rate of discharge by mining and galvanizing industries. The crystalline composition of the transformation products of Cu^{2+} and Fe^0 nanoparticles after the reaction was identified by X-ray diffraction (XRD). The morphologies of the transformed products were analyzed using scanning electron microscopy (SEM) and transmission electron microscopy (TEM), whereas the distribution of elements of the individual morphologies was depicted by TEM mapping. In addition, high-resolution transmission electron microscopy (HR-TEM) was employed to obtain the lattice stripe spacing of individual morphologies, and X-ray photoelectron spectroscopy (XPS) was used to characterize the changes in the valence states of Cu^{2+} and Fe^0 before and after the reaction, thereby confirming the compositional evolution. Subsequently, the mechanism of the compositional evolution of Cu^{2+} and Fe^0 in nZVI was elucidated, and the risk of conversion products was evaluated. Collectively, the above elucidated specific objectives helped to achieve the main objective of the study, which is to provide an insight into the fate of Cu^{2+} and zero-valent iron during Cu^{2+} removal by nZVI.

METHODS

Chemicals

The chemicals used in the study were ferrous sulfate ($FeSO_4•7H_2O$), sodium borohydride ($NaBH_4$) and copper sulfate ($CuSO_4•5H_2O$). All were of analytical grade and obtained from the Tianli Chemical Reagent Company in Tianjin, China. Deionized water was used to prepare the chemical solutions.

Preparation of nZVI

The nanoscale zero-valent iron (nZVI) was prepared under the reduction phase method[16]. First, 13.9 g of iron (II) sulfate heptahydrate ($FeSO_4•7H_2O$) was measured into a beaker, and 50 mL of 0.01 mol/L H_2SO_4 was added. 40 mL of the resulting mixture was pipetted into a three-necked round bottom flask and mechanically stirred (200 rpm) for 5 min. 3.026 g of $NaBH_4$ was measured into a beaker and dissolved with 40 mL of deionized water. The solution was added dropwise into the three-necked round bottom flask and mechanically stirred under N_2 purge. The resulting mixture was allowed to sit and stir mechanically for 15 min after all the $NaBH_4$ solution was used up. The as-prepared nZVI was filtered and washed with deionized water. The material was then dried under vacuum at -30 °C for 14 h in a Freeze Dryer.

Batch experiments

Batch experiments were performed to investigate the transformation of Cu^{2+} and Fe^0 in nZVI after Cu^{2+} removal. First, 200 mL of 5 mmol/L $CuSO_4$ solution was measured into a beaker and the pH of the solution was adjusted to 4.0. The resulting solution was transferred into a 500 mL Erlenmeyer bottle with a stopper and 0.1 g nZVI was added to the solution before reacting in the thermostatic oscillator (200 rpm) at 25 °C. At pre-determined time intervals (5, 10, 20, 30, 45, 60, 90 and 120 min), 2 mL of the mixture was sampled and filtered through a 0.45 μm nitrocellulose membrane. The filtrates obtained at the determined time intervals were analyzed for the removal rate of Cu^{2+}. The batch experiments were performed in duplicate to ensure data precision. The residue of the nZVI after Cu^{2+} removal was vacuum filtered and freeze-dried at -30 °C for 14 h, and then stored in a refrigerator before proceeding to characterize the residue for significant changes in morphology and structure.

Analytical methods

The concentration of Cu^{2+} was analyzed with the aid of the Atomic Absorption Spectrometer (NOVAA-350 Analytic Jena, Germany). Commercial standards of the heavy metal were used to calibrate the equipment and facilitate their identification. The removal efficiency of Cu^{2+} was determined with Equation (1).

Removal efficiency (%) = c_0-c_t/c_0×100%(1)

Where C_0 is the initial concentration of Cu^{2+}, C_t is the concentration of Cu^{2+} at the pre-determined time intervals.

Characterization

The morphological characteristics of the nZVI before and after reaction with Cu^{2+}were analyzed using Scanning Electron Microscopy (SEM) (Nova 400 Nano, FEI, USA) and Transmission Electron Microscopy (TEM) (Tecnai G2 F30, S-Twin, FEI, USA). The condition of measurement for the SEM images was maintained at 1 μm with a 30,000 × magnification. The wavelengths of the TEM images varied and are found at the bottom left corner of each image. The peak at 1.751 keV was omitted in the TEM. The crystalline structure of the samples was also characterized using an X-ray diffractometer (XRD) (D/MAX-2500, Rigaku Co, Japan) operated at 45 kV and 250 mA with CuKα. Continuous scans from 10° to 100° at 2θ were collected with a 0.02° step size and 0.6 s per step count time. The change of valence state and elemental composition of the transformation product formed by the reaction of nZVI and Cu^{2+} were analyzed with the aid of an X-ray Photoelectron Spectrometer (XPS) (Escalab 250Xi, Thermo Fisher Scientific, USA) and a monochromatic Al Kα X-ray source (hν = 1486.6 Ev). The binding energies (BEs) of the samples were calibrated using the C1s peak at 284.8 eV.

RESULTS

Performance of Cu^{2+} removal by nZVI

The removal efficiency of Cu^{2+} by nZVI under the identified reaction conditions is shown in Figure 1 . It is evident that 72.1% of the Cu^{2+} was removed at 5 min, followed by a significant increase in removal till 60 min (100%). The complete removal of the Cu^{2+} ions persisted till 120 min. It is obvious that the reaction conditions support efficient Cu^{2+} removal by nZVI.

Compositional transformation of Cu^{2+} and Fe^0 in nZVI

XRD analyses

The XRD patterns of nZVI before and after the reaction with Cu^{2+} are shown in Figure 2 . The peaks at 44.7°, 65.0° and 82.3° (JCPDS No 06-0696) denoted the presence of Fe^0 in the pristine nZVI spectrum. The Fe^0 peaks in the reacted nZVI spectrum were significantly lower in intensity than those in the pristine nZVI, thus, denoting transformation into iron hydr(oxides). The reacted nZVI spectrum shows that the Fe^0 transformed into goethite (α-FeOOH; 21.2°, 36.6° JCPDS No 81-0463) and lepidocrocite (γ-FeOOH; 27.0°, 36.3°, 46.7° JCPDS No 44-1415) within 120 min. The Cu^{2+} also transformed into copper oxides (cuprite (Cu_2O) and copper metal (Cu^0)) during the removal. The peaks at 29.5°, 36.4°, 42.3°, 61.3°, 73.5°, 77.3° (JCPDS No 05-0667) are indicative of Cu_2O, while those at 43.2°, 50.4°, 74.0°, 89.9° (JCPDS No 04-0836) denote Cu^0.

SEM analyses

Figure 3 shows the SEM images of unreacted nZVI and reacted nZVI. The unreacted nZVI shows the existence of Fe^0 particles which are depicted by the chain-like patterns and aggregated particles due to the magnetic effect of the nZVI [Figure 3A][41,42]. A significant disintegration of the chain-like patterns and subsequent transformation of the morphology after the nZVI reaction with Cu^{2+} are shown in Figure 3B. However, some Fe^0 particles were observed in Figure 3B, as evidenced in the XRD analysis. The crystal morphologies of both Cu_2O and Cu^0 are cubes, thus the morphology of the products of the reaction between nZVI and Cu^{2+} included cubes which can be attributed to Cu_2O (cuprite) and Cu^0 [Figure 3B]. It was reported that lath-like rods are characteristic of lepidocrocite, while twin-rods represent goethite, these two morphologies can be observed in Figure 3B[43].

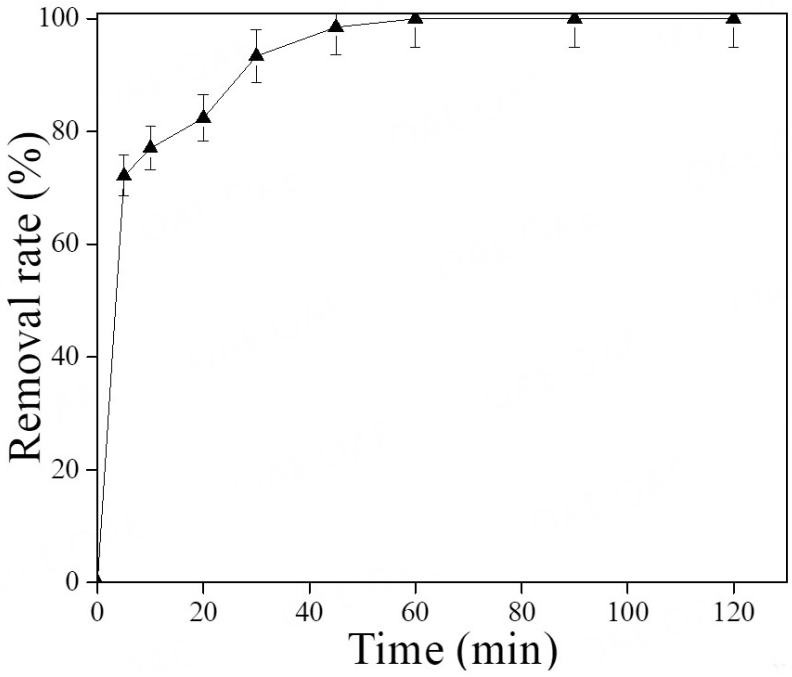

Figure 1. Removal efficiency of Cu^{2+} by nZVI (Reaction conditions: initial concentration = 5 mmol/L; nZVI dosage = 0.5 g/L; initial pH = 4.0 ± 0.1; final pH = 5.1 ± 0.1; temperature = 25 ± 1 °C).

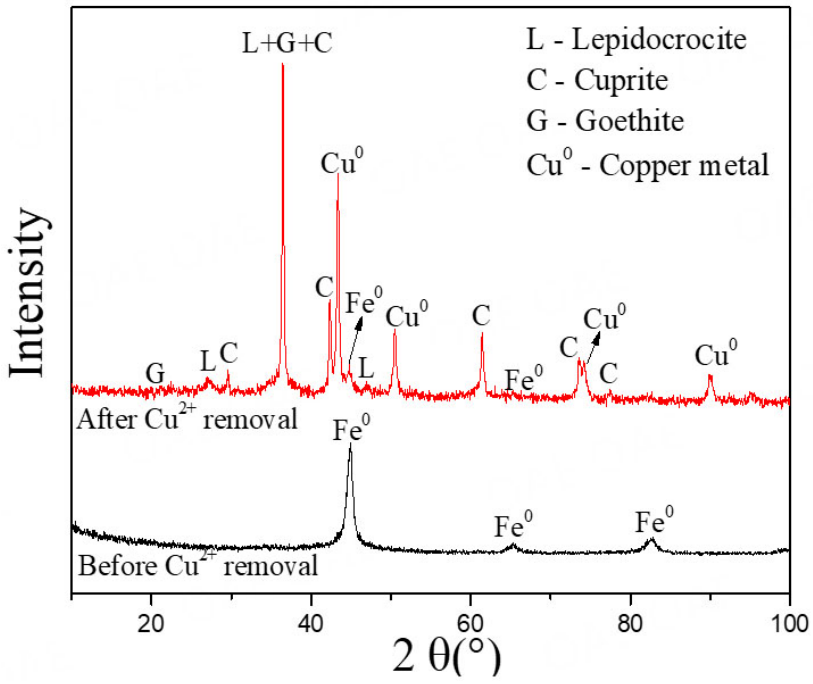

Figure 2. XRD patterns of nZVI before and after reaction with Cu^{2+} showing the transformation of Cu^{2+} and Fe^0 (Reaction conditions: initial concentration = 5 mmol/L; nZVI dosage = 0.5 g/L; initial pH = 4.0 ± 0.1; reaction time = 2 h). XRD: X-ray diffraction.

TEM analyses

The TEM and HR-TEM images of the nZVI reacted with Cu^{2+} are shown in Figure 4. Figures 4A and D

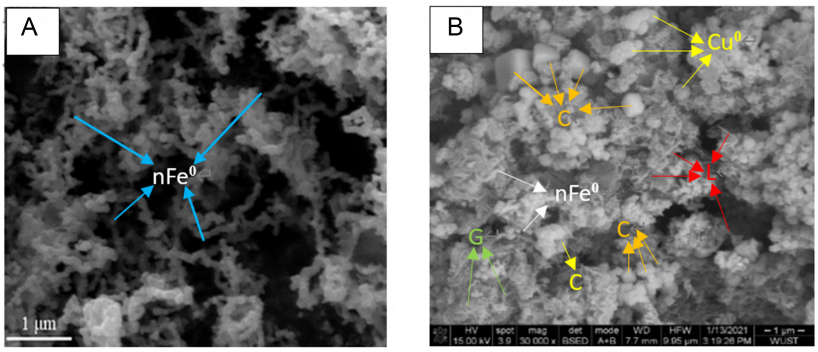

Figure 3. SEM images of pristine nZVI (A) and reacted nZVI (B) (reaction conditions: initial concentration = 5 mmol/L; nZVI dosage = 0.5 g/L; initial pH = 4.0 ± 0.1; reaction time = 2 h.) C: cuprite; G: goethite; L: lepidocrocite; SEM: scanning electron microscopy.

clearly depict the cubic morphology of Cu_2O and Cu^0, which are also confirmed by their corresponding lattice fringes [Figure 4B, C, E, and F]. The lath-like lepidocrocite and twin-rod goethite are also clearly depicted in Figures 4G and J. The lattice fringes in Figure 4H, I, K and L confirm the identified morphologies in the TEM images.

The elemental mapping in Figure 5A was characteristic of cubic morphology. The O and Fe [Figure 5B and 5C] elements were sparsely distributed in the cubic structure, thus, confirming the presence of Cu_2O or Cu^0 in the cubic structure. Considering the elemental mapping in Figure 5A, which is characteristic of cubic morphology, it is observed that more Cu elements were concentrated in the cubic structure [Figure 5D]. On the other hand, the Fe elements in the lath-like morphology were more [Figure 5G] with sparse dispersion of the O elements [Figure 5F]. In the same area, Cu elements were absent [Figure 5H], thus, confirming the presence of lepidocrocite in the lath-like structures in Figure 5E. However, the apparent aggregated morphology in Figure 5E contains more Cu and Fe elements but sparse O elements as depicted in Figures 5F-H. Additionally, the Fe elements were highly distributed in the meshy morphology depicted in Figure 5I, whereas the O and Cu elements were sparsely distributed [Figures 5J and L]. The presence of more Fe elements in Figure 5K coupled with the lattice fringes in Figure 4 reiterates the presence of goethite and lepidocrocite. Moreover, the concentration of Cu elements in the seemingly cubic morphology at the bottom left in Figure 5I denotes Cu^0 and Cu_2O. The results of the elemental mapping are consistent with the analyses of XRD patterns, TEM images and lattice fringes.

XPS analyses

The wide-scan spectra and narrow scan spectra of the nZVI before and after the reaction with the Cu^{2+} are shown in Figure 6 . The wide-scan spectra show the deconvolution of the Cu 2p, Fe 2p and O 1s regions before and after the reaction [Figure 6A]. The Cu 2p spectrum of the pristine nZVI was undefined. However, the nZVI spectrum after Cu^{2+} removal shows the Cu $2p_{3/2}$ and Cu $2p_{1/2}$ peaks at 932.6 eV and 952.4 eV respectively. The Cu $2p_{3/2}$ and Cu $2p_{1/2}$ peaks also denote Cu^0, whereas the peaks at 933.5 eV and 953.2 eV denote Cu_2O [Figure 6B]. The Fe 2p spectrum of the nZVI before Cu^{2+} removal shows Fe^0 (706.7 eV), Fe^{2+} (715.1 eV and 728.0 eV) and Fe^{3+} (719.7 eV and 733.0 eV). The peak intensities of the Fe^{2+} and Fe^{3+} in the nZVI spectrum before Cu^{2+} removal are relatively lower than those in the spectrum after Cu^{2+} removal [Figure 6C]. It is observed that the peak intensity of the Fe^0 in the spectrum after Cu^{2+} removal was low as compared to that in the pristine nZVI. The reduced Fe^0 peak intensity coupled with the increased Fe^{2+} and Fe^{3+} peak intensities denote the transformation of the Fe^0 into more iron hydr(oxides) [Figure 6C]. In addition, it can be observed that the metallic O content in the O 1s region (529.7-530.1 eV) was more in the reacted nZVI as compared to the pristine nZVI, and the organic C-O was evident at 530.9-531.6 eV

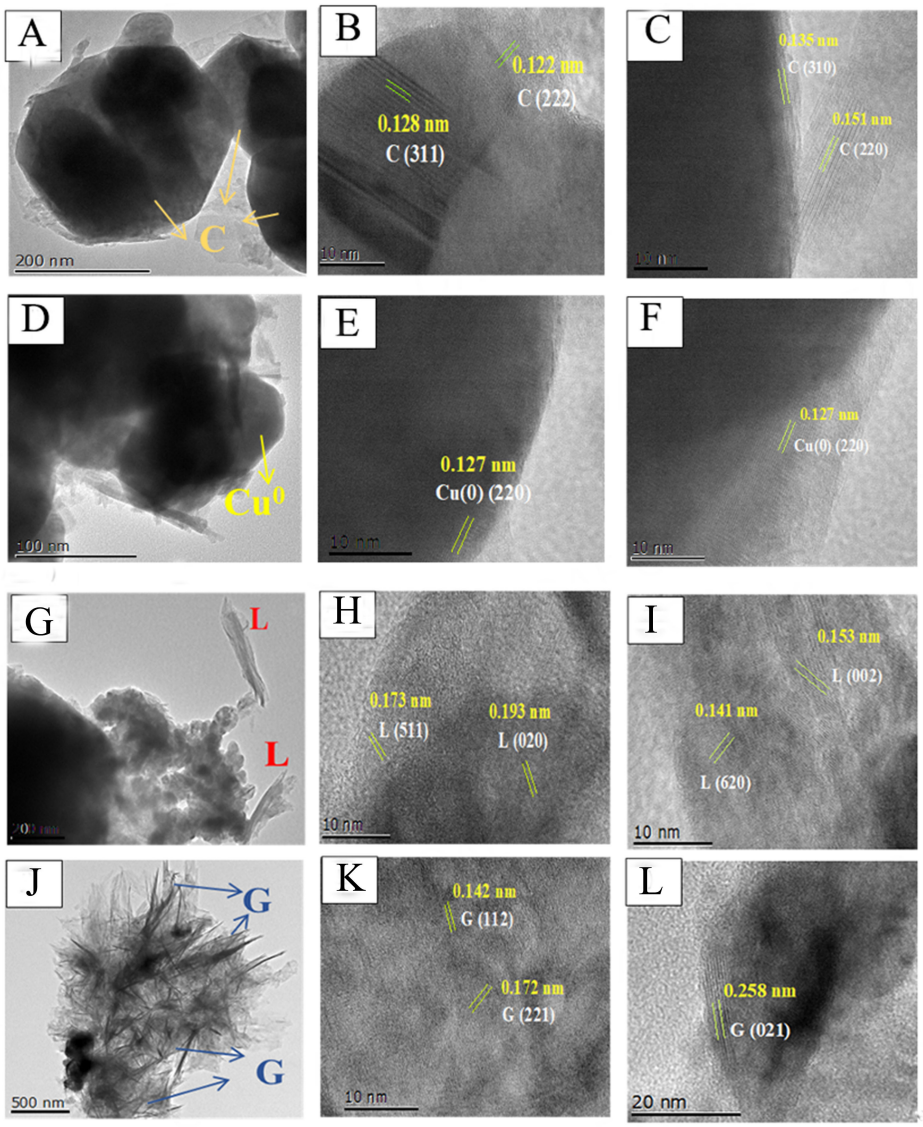

Figure 4. TEM (A, D, G, J) and HR-TEM images (B, C, E, F, H, I, K, I) of nZVI reacted with Cu^{2+} (Reaction conditions: initial concentration = 5 mmol/L; nZVI dosage = 0.5 g/L; temperature = 25 ± 1 °C; initial pH = 4.0 ± 0.1; reaction time = 2 h. C: cuprite; G: goethite; HR-TEM: high-resolution transmission electron microscopy; L: lepidocrocite.

[Figure 6D].

DISCUSSION

Removal of Cu^{2+} by nZVI and transformation of Cu^{2+} and Fe^0 after removal

In this study, complete removal of the Cu^{2+} was achieved within 2 h under pH 4. The finding is similar to that of Xu *et al.*[36], where high removal efficiency of Cu^{2+} was achieved within 2 h. The XRD and XPS patterns in this study were more defined after the 2 h reaction, which can be attributed to the reaction with Cu^{2+}. A comparison of the XRD patterns to that of the lowest pH in Liu *et al.*[44] showed that the rate of ferrihydrite transformation into stable Fe (III) products was low in the absence of Cu^{2+} (an oxidizing agent). It is deduced from the findings of Liu *et al.*[44] that an increase in pH contributes to the effective transformation of the Fe^0 ions in nZVI to Fe(III) products. However, in this study, it can be suggested that the reaction with Cu^{2+} achieves the same fate. Transformation of the Cu^{2+} into Cu_2O/cuprite and Cu^0 is

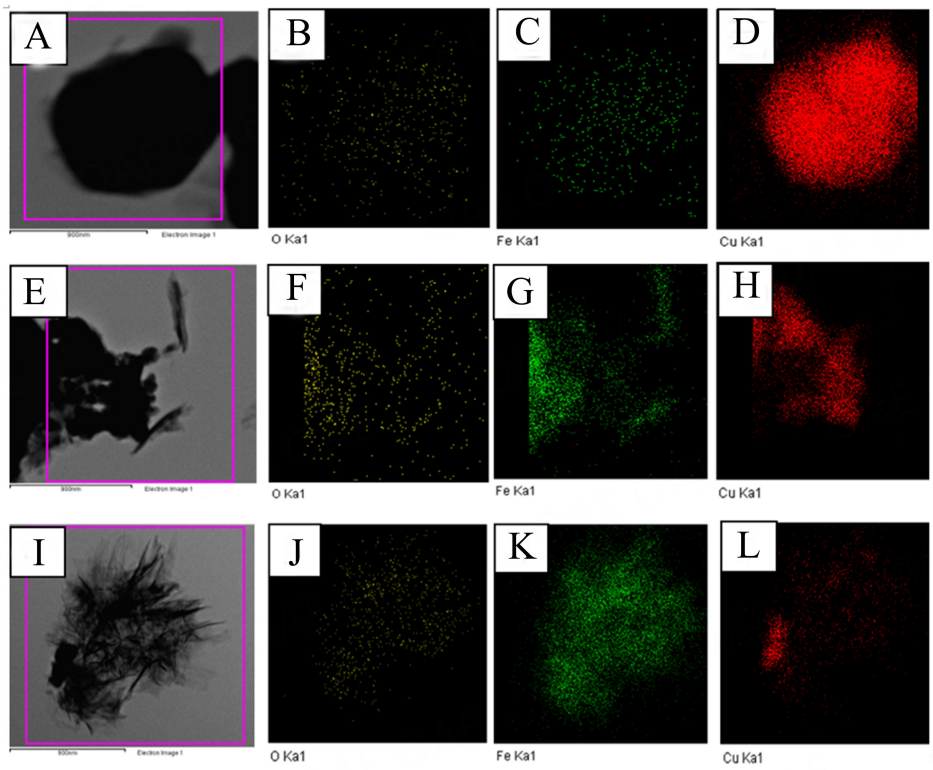

Figure 5. TEM images (A, E, I) and TEM mapping (B, C, D; F, G, H; and J, K, L) of nZVI reacted with Cu^{2+} (initial concentration = 5 mmol/L; nZVI dosage = 0.5 g/L; temperature = 25 ± 1 °C; initial pH = 4.0 ± 0.1; reaction time = 2 h). TEM: transmission electron microscopy.

consistent with Karabelli *et al.*[45]. The results in the TEM and SEM only confirmed the transformations identified in the XRD and XPS[45,46].

Mechanism on transformation of Cu^{2+} and Fe^0 in nZVI

Karabelli *et al.*[45] reported that the removal mechanism of heavy metal ions by nZVI is highly dependent on the redox potential of both parties involved in the reaction. The Fe^0 posed as the reducing agent during the reaction, while the dissolved oxygen (DO, 8.08 mg/L at 25°C), water and Cu^{2+} (the redox potential of Cu^{2+}/Cu is +0.34 V) acted as the oxidizing agents in the removal process. The higher reducibility of the Fe^0 (the redox potential of Fe^{2+}/Fe^0 is -0.44 V) facilitated the reduction of the Cu^{2+} into Cu^0 [Equation 2] and Cu_2O [Equation 3][45-48]. This was validated in the XPS and XRD investigations, where the redox process led to the formation of metallic copper and cuprite on the nZVI surface.

$$Fe^0 + Cu^{2+} \rightarrow Fe^{2+} + Cu^0 \quad (2)$$

$$Fe^0 + 2Cu^{2+} + H_2O \rightarrow Fe^{2+} + Cu_2O + 2H^+ \quad (3)$$

The reduction of the Cu^{2+} by Fe^0 in nZVI influenced the individualistic transformation of Fe^0 into Fe^{2+} [Equations 2 and 3]. Similarly, the reaction of Fe^0 with DO and water influenced the conversion of the Fe^0 into Fe^{2+} [Equation 4]. Hence, while Cu^{2+} undergoes reduction into Cu^0 and Cu_2O, Fe^0 undergoes oxidation into Fe^{2+}. The variation of Fe^{2+} and Fe^{3+} concentrations over time in the reaction process is shown in Supplementary Figure 1. The high Fe^{2+} concentration is proof that the Fe^{2+} promoted corrosion by

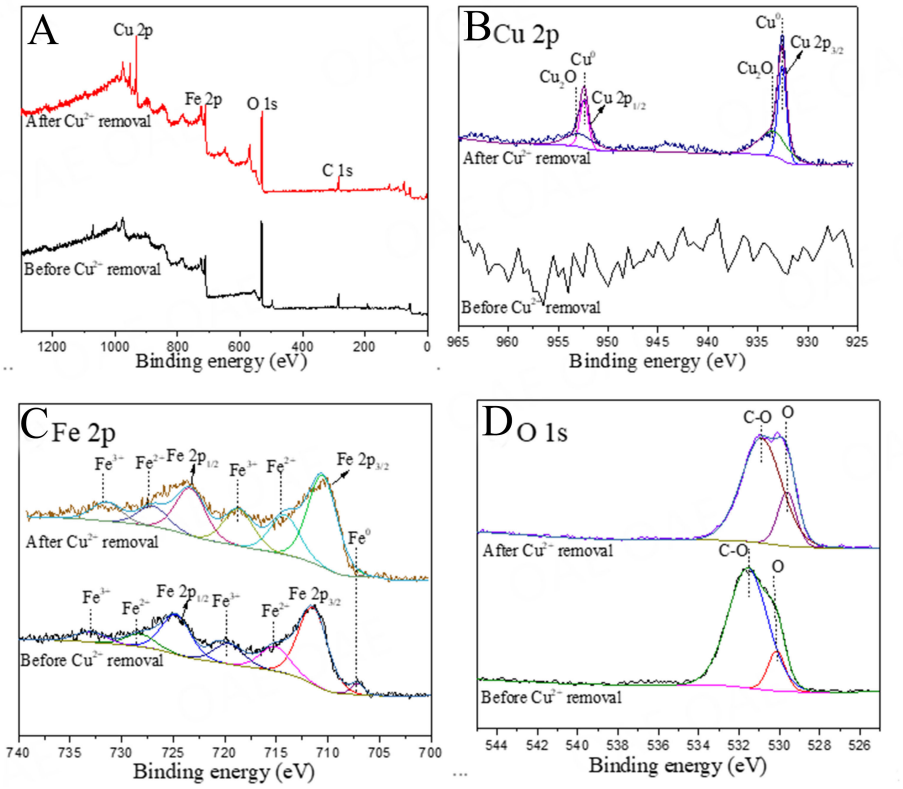

Figure 6. XPS analysis showing the wide scan spectra (A); and narrow scan spectra of Cu2p (B); Fe2p (C) and O1s (D) of nZVI reacted with Cu^{2+} (initial concentration = 5 mmol/L; nZVI dosage = 0.5 g/L; initial pH = 4.0 ± 0.1; temperature = 25 ± 1 °C; reaction time = 2 h). XPS: X-ray photoelectron spectroscopy.

consuming DO, and is responsible for the transformation of amorphous iron hydr(oxides) into stable ones. Thus, eventually affecting the entire electrode process through the cathode.

The formed Fe^{2+} undergoes a series of reactions with OH^-, DO and H_2O till ferrihydrite [$Fe_5O_3(OH)_9$] which is an unstable and amorphous iron oxide is formed [Equations 5-8][39,49,50].

$$2Fe^0 + O_2(aq) + 2H_2O \rightarrow 2Fe^{2+} + 4OH^- \quad (4)$$

$$Fe^{2+} + OH^- \rightarrow Fe(OH)^+ \quad (5)$$

$$Fe(OH)^+ + OH^- \rightarrow Fe(OH)_2 \quad (6)$$

$$4Fe(OH)_2 + O_2(aq) + 2H_2O \rightarrow 4Fe(OH)_3 \quad (7)$$

$$4Fe(OH)_3 + Fe^{2+} \rightarrow Fe_5O_3(OH)_9 + 3H^+ \quad (8)$$

A detailed analysis of the contribution of ferrihydrite to the formation of stable iron oxides upon reaction with the formed Fe^{2+} can be expressed as Equations 9 and 10[50,51], where ferrihydrite is denoted by FhyOH, and the active intermediate formed by FhyOH and Fe^{2+} is denoted by Fhy*OFe$^+$. The formation of lepidocrocite and goethite are expressed in Equations 11 and 12, respectively (in the equations, lepidocrocite

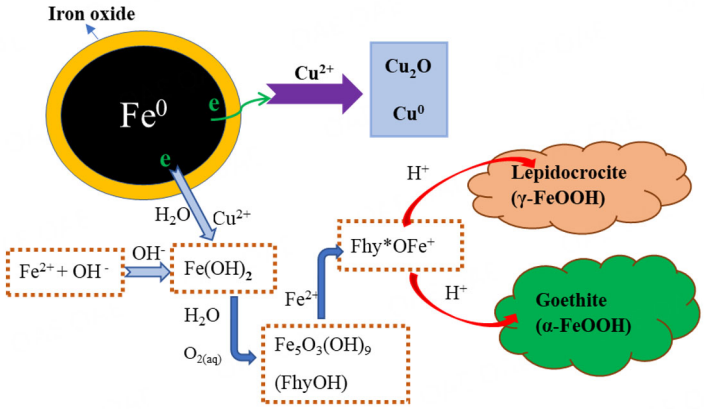

Figure 7. Schematic representation of the transformation of Cu^{2+} and compositional evolution of Fe^0 in nZVI during Cu^{2+} removal.

and goethite are represented by LpdOH and GthOH, respectively).

$$FhyOH + Fe^{2+} \rightarrow Fhy^{*}OFe^{+} + H^{+} \quad (9)$$

$$Fhy^{*}OFe^{+} + H^{+} \rightarrow Fhy^{*}OH + Fe^{2+}(\text{reduced structural } Fe^{3+}) \quad (10)$$

$$Fhy^{*}OFe^{+} + H^{+} \rightarrow LpdOH + Fe^{2+} \quad (11)$$

$$Fhy^{*}OFe^{+} + H^{+} \rightarrow GthOH + Fe^{2+} \quad (12)$$

Based on the findings in this study, Figure 7 was proposed.

The Fe^0 transformation products, lepidocrocite and goethite, have been reported to be less toxic than nZVI in the environment[51,52]. Therefore, the application of nZVI in Cu^{2+} removal does not have the potential to form more toxic substances that could eventually affect human health and the environment. Nonetheless, the accumulation of the transformed products may pose a certain level of threat to biodiversity and humans when the effluent of wastewater treatment is discharged into the environment indiscriminately. Moreover, the LD_{50} for copper oxides has been reported to be > 2,500 mg/kg, while that of Cu^{2+} has been reported to be about 480 mg/kg[53]. Additionally, Cu^{2+} is a dissolved form, which is easy to be taken up and absorbed by aquatic organisms, thus posing a greater threat to the ecosystem. Therefore, the transformation of Cu^{2+} into copper oxides is beneficial to the environment and poses a relatively lower threat to human and environmental health as compared to Cu^{2+} in the environment.

In conclusion, this study investigated the methodic transformation of Cu^{2+} and Fe^0 during Cu^{2+} removal by nZVI. The results showed that complete removal of Cu^{2+} by nZVI was achieved within 60 min and remained constant till the 120 min reaction time. The removal process of Cu^{2+} resulted in the transformation of the Cu^{2+} into Cu^0 and Cu_2O with cubic crystal morphology, thus iterating that the mechanism of Cu^{2+} transformation is attributed to the reduction of Fe^0. Moreover, the Fe^0 particles transformed into lath-like lepidocrocite and twin-rod goethite. The mechanism of nZVI transformation is that Fe^0 in nZVI reacts with Cu^{2+}, water and dissolved oxygen to form Fe^{2+} and ferrihydrite first, and then ferrihydrite reacts with Fe^{2+} and H^+ to form lepidocrocite and goethite. Cu^0, Cu_2O, lepidocrocite and goethite are solid metallic minerals with relatively low biological availability in the environment. Therefore, the

removal of Cu^{2+} by nZVI is an environmentally friendly wastewater treatment/groundwater remediation technology that has the potential for wide-scale application. For future studies, a simulation of the applicability of nZVI in removing Cu^{2+} on a large scale can be done along with a cost-benefit analysis.

DECLARATIONS

Acknowledgments

The authors would like to thank the Analytical and Testing Center, Wuhan University of Science and Technology for helpful contributions in the execution of this study.

Authors' contributions

Made substantial contributions to the conception of the study, performed data analysis and investigation, synthesized material, curated data and wrote the first draft: Anang E

Made substantial contributions to the conception of the study, supervised the experiments, reviewed and edited the manuscript: Liu H

Performed software edits, reviewed and edited the manuscript, and provided technical and material support: Fan X

Availability of data and materials

All data pertinent to the study are included in the manuscript

Financial support and sponsorship

The authors would like to express their gratitude to the Key Project of the Natural Science Foundation of China (Grant No. 41230638) for the financial support; The support from the Open Fund of Hubei Key Laboratory for Efficient Utilization and Agglomeration of Metallurgic Mineral Resources from Wuhan University of Science and Technology (2017zy008) is duly acknowledged.

Conflicts of interest

All authors declared that there are no conflicts of interest.

Ethical approval and consent to participate

Not applicable.

Consent for publication

Not applicable.

REFERENCES

1. Gautam PK, Gautam RK, Banerjee S, Chattopadhyaya MC, Pandey JD. Heavy metals in the environment: fate, transport, toxicity and remediation technologies. Available from: https://www.researchgate.net/publication/314465070 [Last accessed on 27 Mar 2023].
2. Liu J, Liu YJ, Liu Y, Liu Z, Zhang AN. Quantitative contributions of the major sources of heavy metals in soils to ecosystem and human health risks: a case study of Yulin, China. *Ecotoxicol Environ Saf* 2018;164:261-9. DOI PubMed
3. Ali I, Burakov AE, Melezhik AV, Babkin AV, Burakova IV, Neskomornaya ME, Galunin EV, Tkachev AG, Kuznetsov DV. Removal of copper(II) and zinc(II) ions in water on a newly synthesized polyhydroquinone/graphene nanocomposite material: kinetics, thermodynamics and mechanism. *ChemistrySelect* 2019;4:12708-18. DOI
4. Liang W, Dai C, Zhou X, Zhang Y. Application of zero-valent iron nanoparticles for the removal of aqueous zinc ions under various experimental conditions. *PLoS One* 2014;9:e85686. DOI PubMed PMC
5. Madhu PM, Sadagopan RS. Effect of heavy metals on growth and development of cultivated plants with reference to cadmium, chromium and lead–a review. Available from: https://cyberleninka.ru/article/n/effect-of-heavy-metals-on-growth-and-development-of-

cultivated-plants-with-reference-to-cadmium-chromium-and-lead-a-review [Last accessed on 27 Mar 2023].
6. Ali J, Khan S, Khan A, Waqas M, Nasir MJ. Contamination of soil with potentially toxic metals and their bioaccumulation in wheat and associated health risk. *Environ Monit Assess* 2020;192:138. DOI PubMed
7. Sandeep G, Vijayalatha KR, Anitha T. Heavy metals and its impact in vegetable crops. Available from: https://www.researchgate.net/publication/341508109 [Last accessed on 27 Mar 2023].
8. Panfili I, Bartucca ML, Ballerini E, Del Buono D. Combination of aquatic species and safeners improves the remediation of copper polluted water. *Sci Total Environ* 2017;601-602:1263-70. DOI PubMed
9. Ho YS. Removal of copper ions from aqueous solution by tree fern. *Water Res* 2003;37:2323-30. DOI PubMed
10. Yan W, Ramos MAV, Koel BE, Zhang W. As(III) sequestration by iron nanoparticles: study of solid-phase redox transformations with X-ray photoelectron spectroscopy. *J Phys Chem C* 2012;116:5303-11. DOI
11. Aydin H, Bulut Y, Yerlikaya C. Removal of copper (II) from aqueous solution by adsorption onto low-cost adsorbents. *J Environ Manage* 2008;87:37-45. DOI PubMed
12. Thanh DN, Novák P, Vejpravova J, Vu HN, Lederer J, Munshi T. Removal of copper and nickel from water using nanocomposite of magnetic hydroxyapatite nanorods. *J Magn Magn Mater* 2018;456:451-60. DOI
13. Hosseinzadeh H, Ramin S. Effective removal of copper from aqueous solutions by modified magnetic chitosan/graphene oxide nanocomposites. *Int J Biol Macromol* 2018;113:859-68. DOI PubMed
14. Wang L, Li J, Wang J, et al. Green multi-functional monomer based ion imprinted polymers for selective removal of copper ions from aqueous solution. *J Colloid Interface Sci* 2019;541:376-86. DOI PubMed
15. Stefaniuk M, Oleszczuk P, Ok YS. Review on nano zerovalent iron (nZVI): from synthesis to environmental applications. *Chem Eng J* 2016;287:618-632. DOI
16. Mukherjee R, Kumar R, Sinha A, Lama Y, Saha AK. A review on synthesis, characterization, and applications of nano zero valent iron (nZVI) for environmental remediation. *Crit Rev Env Sci* 2015;46:443-66. DOI
17. Li S, Yang F, Li J, Cheng K. Porous biochar-nanoscale zero-valent iron composites: Synthesis, characterization and application for lead ion removal. *Sci Total Environ* 2020;746:141037. DOI PubMed
18. Navaei Diva T, Zare K, Taleshi F, Yousefi M. Removal of $Cd2^{+}$ from aqueous solution by nickel oxide/CNT nanocomposites. Available from:https://scholar.google.com.hk/scholar?q=Removal+of+Cd2%2B+from+Aqueous+Solution+by+Nickel+Oxide/CNT+Nanocomposites&hl=zh-CN&as_sdt=0&as_vis=1&oi=scholart [Last accessed on 27 Mar 2023].
19. Lian JJ, Yang M, Wang HL, et al. Enhanced molybdenum(VI) removal using sulfide-modified nanoscale zerovalent iron: kinetics and influencing factors. *Water Sci Technol* 2021;83:297-308. DOI PubMed
20. Zhao Y, Zhao Z, Song X, et al. Effects of nZVI dosing on the improvement in the contaminant removal performance of constructed wetlands under the dye stress. *Sci Total Environ* 2020;703:134789. DOI PubMed
21. Liu J, Liu A, Wang W, Li R, Zhang WX. Feasibility of nanoscale zero-valent iron (nZVI) for enhanced biological treatment of organic dyes. *Chemosphere* 2019;237:124470. DOI PubMed
22. Wei A, Ma J, Chen J, Zhang Y, Song J, Yu X. Enhanced nitrate removal and high selectivity towards dinitrogen for groundwater remediation using biochar-supported nano zero-valent iron. *Chem Eng J* 2018;353:595-605. DOI
23. Han L, Li B, Tao S, et al. Graphene oxide-induced formation of a boron-doped iron oxide shell on the surface of nZVI for enhancing nitrate removal. *Chemosphere* 2020;252:126496. DOI PubMed
24. Cao Y, Zhang S, Zhong Q, et al. Feasibility of nanoscale zero-valent iron to enhance the removal efficiencies of heavy metals from polluted soils by organic acids. *Ecotoxicol Environ Saf* 2018;162:464-73. DOI PubMed
25. Huang P, Ye Z, Xie W, et al. Rapid magnetic removal of aqueous heavy metals and their relevant mechanisms using nanoscale zero valent iron (nZVI) particles. *Water Res* 2013;47:4050-8. DOI PubMed
26. Calderon B, Fullana A. Heavy metal release due to aging effect during zero valent iron nanoparticles remediation. *Water Res* 2015;83:1-9. DOI PubMed
27. Liang L, Li X, Guo Y, Lin Z, Su X, Liu B. The removal of heavy metal cations by sulfidated nanoscale zero-valent iron (S-nZVI): The reaction mechanisms and the role of sulfur. *J Hazard Mater* 2021;404:124057. DOI PubMed
28. Lei C, Sun Y, Khan E, et al. Removal of chlorinated organic solvents from hydraulic fracturing wastewater by bare and entrapped nanoscale zero-valent iron. *Chemosphere* 2018;196:9-17. DOI PubMed
29. Li Q, Chen Z, Wang H, et al. Removal of organic compounds by nanoscale zero-valent iron and its composites. *Sci Total Environ* 2021;792:148546. DOI PubMed
30. Xu L, Wang J. A heterogeneous fenton-like system with nanoparticulate zero-valent iron for removal of 4-chloro-3-methyl phenol. *J Hazard Mater* 2011;186:256-64. DOI PubMed
31. Abbas T, Wadhawan T, Khan A, McEvoy J, Khan E. Virgin (Fe^{0}) and microbially regenerated (Fe^{2+}) iron turning waste for treating chlorinated pesticides in water. *J Hazard Mater* 2020;398:122980. DOI
32. Malakootian M, Daneshkhah M, Hossaini H. Removal of phosphates from aqueous solution by sepiolite-nano zero valent iron composite optimization with response surface methodology. *Int J Environ Sci Te* 2017;15:2129-40. DOI
33. Pasinszki T, Krebsz M. Synthesis and Application of Zero-Valent Iron Nanoparticles in Water Treatment, Environmental Remediation, Catalysis, and Their Biological Effects. *Nanomaterials* 2020;10:917. DOI PubMed PMC
34. O'Carroll D, Sleep B, Krol M, Boparai H, Kocur C. Nanoscale zero valent iron and bimetallic particles for contaminated site remediation. *Adv Water Resour* 2013;51:104-22. DOI

35. Filip J, Kolařík J, Petala E, Petr M, Šráček O, Zbořil R. Nanoscale zerovalent iron particles for treatment of metalloids. In: Phenrat T, Lowry GV, editors. Nanoscale Zerovalent Iron Particles for Environmental Restoration. Cham: Springer International Publishing; 2019. pp. 157-99. DOI
36. Xu W, Hu X, Lou Y, et al. Effects of environmental factors on the removal of heavy metals by sulfide-modified nanoscale zerovalent iron. *Environ Res* 2020;187:109662. DOI PubMed
37. Dai C, Zhou Z, Zhou X, Zhang Y. Removal of Sb(III) and Sb(V) from aqueous solutions using nZVI. *Water Air Soil Poll* 2013:225. DOI
38. Wen Z, Zhang Y, Dai C. Removal of phosphate from aqueous solution using nanoscale zerovalent iron (nZVI). *Colloid Surface A* 2014;457:433-40. DOI
39. Anang E, Liu H, Fan X, Zhao D, Gong X. Compositional evolution of nanoscale zero valent iron and 2,4-dichlorophenol during dechlorination by attapulgite supported Fe/Ni nanoparticles. *J Hazard Mater* 2021;412:125246. DOI PubMed
40. Yang L, Steefel CI, Marcus MA, Bargar JR. Kinetics of Fe(II)-catalyzed transformation of 6-line ferrihydrite under anaerobic flow conditions. *Environ Sci Technol* 2010;44:5469-75. DOI PubMed
41. He F, Zhao D, Liu J, Roberts CB. Stabilization of Fe− Pd nanoparticles with sodium carboxymethyl cellulose for enhanced transport and dechlorination of trichloroethylene in soil and groundwater. *Ind Eng Chem Res* 2007;46:29-34. DOI
42. Cheng S, Liu H, Anang E, Li C, Fan X. Enhanced as(III) sequestration using nanoscale zero-valent iron modified by combination of loading and sulfidation: characterizations, performance, kinetics and mechanism. *Water Sci Technol* 2021;83:2886-900. DOI PubMed
43. Cornell R. M., Schwertmann U. John Wiley & Sons 2003. The iron oxides: structure, properties, reactions, occurrences and uses. DOI
44. Liu H, Li P, Zhu M, Wei Y, Sun Y. Fe(II)-induced transformation from ferrihydrite to lepidocrocite and goethite. *J Solid State Chem* 2007;180:2121-8. DOI
45. Karabelli D, Üzüm C, Shahwan T, Eroglu AE, Scott TB, Hallam KR, Lieberwirth I. Batch removal of aqueous $Cu2^{+}$ ions using nanoparticles of zero-valent iron: a study of the capacity and mechanism of uptake. *Ind Eng Chem Res* 2008;47:4758-64. DOI
46. Karabelli D, Ünal S, Shahwan T, Eroğlu AE. Preparation and characterization of alumina-supported iron nanoparticles and its application for the removal of aqueous $Cu2^{+}$ ions. *Chem Eng J* 2011;168:979-84. DOI
47. Tarekegn MM, Hiruy AM, Dekebo AH. Correction: nano zero valent iron (nZVI) particles for the removal of heavy metals (Cd^{2+}, Cu^{2+} and Pb^{2+}) from aqueous solutions. *RSC Adv* 2021;11:27084. DOI
48. Zhou YT, Branford-White C, Nie HL, Zhu LM. Adsorption mechanism of $Cu2^{+}$ from aqueous solution by chitosan-coated magnetic nanoparticles modified with alpha-ketoglutaric acid. *Colloids Surf B Biointerfaces* 2009;74:244-52. DOI PubMed
49. Aeppli M, Kaegi R, Kretzschmar R, Voegelin A, Hofstetter TB, Sander M. Electrochemical analysis of changes in iron oxide reducibility during abiotic ferrihydrite transformation into goethite and magnetite. *Environ Sci Technol* 2019;53:3568-78. DOI PubMed
50. Chen C, Kukkadapu R, Sparks DL. Influence of coprecipitated organic matter on $Fe2^{+}$(aq)-catalyzed transformation of ferrihydrite: implications for carbon dynamics. *Environ Sci Technol* 2015;49:10927-36. DOI PubMed
51. Perez JP, Tobler DJ, Thomas AN, Freeman HM, Dideriksen K, Radnik J, Benning LG. Adsorption and reduction of arsenate during the Fe2+-induced transformation of ferrihydrite. *Acs Earth Space Chem* 2019;3:884-94. DOI
52. Bardos P, Bone B, Daly P, Elliot D, Jones S, Lowry G, Merly C. A risk benefit appraisal for the application of nanoscale zero valent iron (nZVI) for the remediation of contaminated sites. Available from: https://www.researchgate.net/publication/264788812 [Last accessed on 27 Mar 2023].
53. Elkhateeb SA, Ibrahim TR, El-Shal AS, Abdel Hamid OI. Ameliorative role of curcumin on copper oxide nanoparticles-mediated renal toxicity in rats: an investigation of molecular mechanisms. *J Biochem Mol Toxicol* 2020;34:e22593. DOI PubMed